



Article

Evaluation of BDS-3 B1C/B2b Single/Dual-Frequency PPP Using PPP-B2b and RTS SSR Products in Both Static and Dynamic Applications

Ruohua Lan, Cheng Yang ^{*}, Yanli Zheng, Qiaozhuang Xu, Jie Lv and Zhouzheng Gao

School of Land Science and Technology, China University of Geosciences Beijing, Beijing 100083, China

* Correspondence: c.yang@connect.polyu.hk; Tel.: +86-157-1284-7511

Abstract: The BeiDou Global Navigation Satellite System (BDS-3) can provide PPP-B2b satellite-based Precise Point Positioning (PPP) real-time service to the Asia-Pacific region via PPP-B2b signal transmitted from the three Geostationary Earth Orbit (GEO) satellites. This paper provides a comprehensive evaluation of the accuracies of the satellite's precise real-time orbit and clock products, including BDS-3 PPP-B2b precise products and the precise real-time products provided by four IGS centers (CAS, DLR, GFZ, and WHU). In addition, the influences of these real-time precise satellite products on the PPP positioning accuracy with single-frequency and dual-frequencies are also studied. Furthermore, the accuracies of broadcast ephemeris and IGS ultra-rapid products are studied, as well as their impact on PPP accuracies. Results illustrate that the orbits accuracies of PPP-B2b orbits are 9.42 cm, 21.26 cm, and 28.65 cm in the radial, along-track, and cross-track components, which are slightly lower than those of real-time orbits provided by the four IGS centers. However, the accuracy of PPP-B2b clock biases is 0.18 ns, which is higher than those provided by IGS Real-Time Service (RTS). In the static positioning test, the 3D positioning accuracy of B1I+B3I dual-frequencies PPP and B1C single-frequency PPP are centimeter-level while using PPP-B2b service, which is slightly lower in horizontal components compared to those obtained based on IGS RTS products. The results of the dynamic vehicle test indicate that the positioning accuracies of B1I+B2b dual-frequency PPP are about 50 cm and 120 cm in horizontal and vertical components, which are close to those of B2b single-frequency PPP using PPP-B2b service. Generally, the PPP-B2b orbit and clock accuracies on real-time PPP present similar performance to that based on IGS RTS.

Keywords: PPP-B2b service; BDS-3 new signals; RT-PPP; single-/dual-frequency RT-PPP



Citation: Lan, R.; Yang, C.; Zheng, Y.; Xu, Q.; Lv, J.; Gao, Z. Evaluation of BDS-3 B1C/B2b Single/Dual-Frequency PPP Using PPP-B2b and RTS SSR Products in Both Static and Dynamic Applications. *Remote Sens.* **2022**, *14*, 5835. <https://doi.org/10.3390/rs14225835>

Academic Editors: Giuseppe Casula, Zhetao Zhang and Wenkun Yu

Received: 18 October 2022

Accepted: 14 November 2022

Published: 17 November 2022

Publisher's Note: MDPI stays neutral with regard to jurisdictional claims in published maps and institutional affiliations.



Copyright: © 2022 by the authors. Licensee MDPI, Basel, Switzerland. This article is an open access article distributed under the terms and conditions of the Creative Commons Attribution (CC BY) license (<https://creativecommons.org/licenses/by/4.0/>).

1. Introduction

The 3rd generation of the BeiDou Global Navigation Satellite System (BDS-3) officially provides services of Positioning, Navigation, and Timing (PNT) to global users as of 31 July 2020. The BDS-3 constellation consists of 30 satellites, including 24 Medium Earth Orbit (MEO) satellites, 3 Geostationary Earth Orbit (GEO) satellites, and 3 Inclined Geosynchronous Satellite Orbit (IGSO) satellites [1–3]. In addition to the standard PNT services provided by GPS, Galileo, and GLONASS, BDS-3 is the first system that provides short message communication services and Precise Point Positioning (PPP) real-time service. Real-Time Kinematic (RTK) and PPP are the most widely applied high-accuracy positioning techniques. The RTK positioning accuracy, however, declines along with the increasing baseline, and the conventional Real-time PPP (RT-PPP) based on the real-time orbit/clock products of the International GNSS Service (IGS) is limited by the internet connection. The RT-PPP service provided by BDS-3 uses the B2b (1207.14 MHz) signal to broadcast the orbit and clock corrections directly.

The PPP positioning accuracy is highly related to the satellite orbits and clocks accuracies, which are mainly obtained from the IGS [4–7]. However, IGS final products are

generated with a two-week delay, and the IGS fast orbit and clock products are seven-teen hours delayed. To fulfill the RT-PPP applications, IGS started providing ultra-rapid products on 3 November 2000, with centimeter to decimeter-level accuracy [8–12]. The IGS ultra-rapid files involve 24 h of properly arranged orbit and clock ephemerides. The first 24 h of each IGS ultra-rapid orbit and clock information is estimated from the latest observations from the IGS hourly tracking network. The second 24 h of data are the predicted orbits and clocks, which are extrapolated from the formerly observed orbits. To satisfy the growing demand for real-time high-precision applications (such as precision agriculture, earthquake warning, and tsunami warning) [13], IGS established a real-time working group to provide GPS/GLONASS orbit and clock corrections based on RTCM for the RT-PPP service [14,15]. Currently, IGS analysis centers (ACs), such as GFZ (Deutsches GeoForschungs Zentrum), WHU (Wuhan University), and CAS (Chinese Academic of Science), provide real-time orbits and clock products. The types of precise products and related constellations provided by different IGS centers are presented in Table 1.

Table 1. The IGS SSR message information and the corresponding interval.

IGS Center	Orbit	Clock	Code Bias	Phase Bias	VTEC	GNSS
BKG	60 s	5 s	60 s	60 s	-	G/R/E
CAS	5 s	5 s	10 s	-	60 s	G/R/E/C
CNES	5 s	5 s	5 s	5 s	60 s	G/R/E/C
DLR	30 s	5 s	30 s	30 s	-	G/R/E/C/J ¹
GFZ	5 s	5 s	5 s	-	-	G/R/E/C
WHU	5 s	5 s	-	-	-	G/R/E/C

¹ G, R, E, C, and J denote GNSS, GOLANSS, Galileo, BDS, and Quasi-Zenith Satellite System (QZSS), respectively.

Scholars have evaluated the accuracies of different IGS ACs' real-time products and their impact on the RT-PPP. Elsobeiey and Al-Harbi [16] analyzed the RT-PPP accuracies based on the global IGS stations using the IGS ultra-rapid products and real-time service (RTS). The results show that using the RT-PPP based on the IGS RTS can provide 50% position improvements compared to ultra-rapid products in terms of the Root Mean Square Error (RMSE). Li et al. [17] implemented a network RT-PPP model based on RTKLIB software and further evaluated the mode using both static and kinematic GPS experiments observations. According to the static positioning results, the horizontal and the vertical components achieved centimeter-level accuracy, while the kinematic RT-PPP achieved decimeter-level in those components. The quality of GPS/GLONASS/BDS-2/Galileo quad-system SSR products from eight different IGS analysis centers was evaluated by Wang et al. [18]. The study indicated that the RMSE between GPS real-time orbit and final precise orbit was centimeter level for all ACs, in which the Standard Deviation (STD) of the GPS clock was within 0.3 ns. The GLONASS orbit RMSE was also centimeter level, and the clock STD was twice large as that of GPS. The BDS and Galileo orbit accuracies from CNES were about 14.54 cm and 4.42 cm, respectively, and the clock accuracies of those two constellations were 0.32 ns and 0.18 ns, respectively. The study further studied the real-time product accuracy influences on the kinematic PPP with both simulation and field tests. The positioning results from the studied IGS ACs were centimeter level in horizontal and vertical components, respectively. The kinematic RT-PPP field test indicates that the positioning accuracies estimated by CNES' real-time products were better than those based on CAS precise products. Ouyang et al. [19] studied the performance of BDS-2 real-time products from four IGS centers, WHU, CNES, DLR, and GFZ. The availabilities of all these real-time products were more than 85%, and the real-time orbit accuracies of the GEO and IGSO/MEO satellites were meter level and decimeter level, respectively. Among all of these products, CNES provided the highest accuracy on 3D orbit and clock products. In static PPP mode, the convergence time on average was less than 1.5 h with 11.0 cm positioning accuracy, while in the kinematic mode, the convergence time was 2.11 h~9.84 h with 30.7 cm~68.0 cm positioning accuracy. Ge et al. [20] evaluated the accuracy availability of the BDS-3 real-time products from CENS using continuous data of 41 days. The results

showed that satellite orbit accuracies were about 6 cm in radial and cross-track components but more than 10 cm in the along-track component, and the accuracy of the clock was 0.46 ns. The BDS-3 real-time product availability from CENS is over 80%. The PPP positioning errors in static were within 3 cm at East (E), North (N), and Up (U) components, which was comparable to that of GPS RT-PPP.

Different from the internet-based RT-PPP service provided by the IGS, BDS-3 broadcasts the correction of satellite orbit and clock for both BDS-3 and GPS via the PPP-B2b signal. Simultaneously, the BDS-3 Differential Code Bias (DCB) is broadcast to facilitate dual-frequency PPP positioning applications [3]. Table 2 lists the broadcast PPP-B2b correction messages [21–23].

Table 2. The PPP-B2b message information.

Information	Message Type	Sample Rate (s)	Nominal Validity (s)
Satellite mask	1	48	-
Orbit correction and User range accuracy	2	48	96
Differential code bias	3	48	86,400
Clock correction	4	6	12

The performance evaluations of PPP-B2b products have gained interest from researchers recently. Yang et al. [3] presented the positioning accuracy evaluation of dual-frequency B1C/B2a PPP with Ionosphere-Free (IF) combination based on the PPP-B2b data from 1 August to 30 November 2020. The results indicated that about 30 cm and 50 cm positioning accuracies in the horizontal and vertical components could be achieved with a 30 min convergence time. Lu et al. [21] analyzed the accuracy, integrity, and stability of the orbit clock and DCB corrections of both BDS and GPS provided by the BDS-3 PPP-B2b signal, which proved that the PPP-B2b signal could provide stable and accurate PPP services in China and surrounding areas. Nie et al. [22] compared the orbits and clocks accuracies between PPP-B2b corrections and GFZ final products with three days of observation. The BDS-3 satellite orbit accuracies in radial, along-track, and cross-track components are about ten centimeters, and the BDS-3 clock accuracy was centimeter-level. The static PPP with PPP-B2b correction messages achieved centimeter-level accuracy in the E, N, and U components, and the kinematic PPP of those also achieved centimeter-level accuracy. Tao et al. [23] illustrated that the real-time BDS-3 PPP-B2b correction messages presented better availability and integrity than CNES on BDS satellites. The positioning accuracy of PPP-B2b products-based BDS-3 kinematic PPP can achieve centimeter-level. Xu et al. [24] provided an extensive evaluation of the RT-PPP performance of the PPP-B2b products in terms of matching characteristics, product accuracies, and availability. The results showed that the RMSE of the MEO satellite orbit in radial, along-track, and cross-track components were 6.8 cm, 33.4 cm, and 36.6 cm, respectively, and the accuracy of the clock was 0.2 ns. The availability of BDS-3 PPP-B2b products is over 80%. The PPP test results presented that the accuracies of BDS-3 dual-frequency kinematic RT-PPP after convergence were 11 cm and 17 cm in horizontal and vertical components. In addition, the positioning accuracy of the B1C/B2a IF combination PPP was better than that of the B1I/B3I IF PPP. Ren et al. [25] evaluated the accuracy of PPP-B2b products and the corresponding RT-PPP, and the results showed that the real-time orbit accuracy is about 7.25, 24.79, and 25.87 cm in radial, along-track, and cross-track components for BDS-3 satellites, and 7.29, 30.98, and 21.93 cm for those of GPS satellites. The STD of the clock offset errors for BDS-3 and GPS are within 0.2 ns and 0.15 ns, respectively. The positioning accuracy of real-time BDS+GPS integrated static PPP was about 1.07 cm, 2.69 cm, and 2.25 cm in the N, E, and U directions, and the kinematic PPP of those were about 3.6 cm, 5.9 cm, and 9.4 cm in the N, E, and U directions.

Earlier studies evaluated the PPP-B2b performance using the dual-frequency PPP with static and simulated kinematic mode. However, the PPP-B2b RT-PPP based on the practical kinematic data has hardly been studied, especially using the BDS-3 new signals

(B1C and B2b). Therefore, this contribution will present a comprehensive performance evaluation on the real-time orbit and clock products provided by broadcast ephemeris, BDS-3 PPP-B2b, CAS, DLR, GFZ, and WHU, as well as the ultra-rapid products from WHU. The performance of the kinematic dual-and single-frequency RT-PPP is analyzed with B1C+B2b observation data collected in Beijing, China. The paper is arranged as follows. The recovery method of real-time orbit and clock offset and the mathematical models of dual-/single-frequency PPP are described in the next section. Then, the accuracy of the orbit and clock offset provided by broadcast ephemeris, PPP-B2b, CAS, DLR, GFZ, and WHU are evaluated separately. The positioning accuracy with dual-/single-frequency real-time dynamic PPP is afterward assessed, and the conclusions about the accuracy of real-time satellite orbit and clock products and their impacts on dual-/single-frequency PPP are drawn.

2. Methodologies

The recovery methods of PPP-B2b real-time orbit and clock, the evaluation principle, and the models of real-time dual-frequency and single-frequency PPP are presented in this section.

2.1. PPP-B2b Orbit Recovery

BDS-3 PPP-B2b orbit and clock products are corrections with respect to the broadcast ephemeris. The orbit correction coordinate is related to the satellite-fixed coordinate system in radial, along-track, and cross-track directions. The satellite positions used for PPP, however, are located in the ECEF frame. Thus, the orbit corrections should be transformed into the ECEF system to correct the satellite positions from the broadcast ephemeris [26]. The corrected real-time precise satellite position can be expressed as,

$$\begin{bmatrix} X \\ Y \\ Z \end{bmatrix}_t = \begin{bmatrix} X_{brdc} \\ Y_{brdc} \\ Z_{brdc} \end{bmatrix}_t - \mathbf{R} \cdot \begin{bmatrix} \Delta_r \\ \Delta_a \\ \Delta_c \end{bmatrix}_t \quad (1)$$

With

$$\mathbf{R} = \begin{bmatrix} \frac{\dot{r}}{|\dot{r}|} \times \frac{r \times \dot{r}}{|r \times \dot{r}|} & \frac{\dot{r}}{|\dot{r}|} & \frac{r \times \dot{r}}{|r \times \dot{r}|} \end{bmatrix} \quad (2)$$

where Δ_r , Δ_a and Δ_c represent the position corrections in the radial, along-track, and cross-track directions, respectively; $[X \ Y \ Z]^T$ and $[X_{brdc} \ Y_{brdc} \ Z_{brdc}]^T$ represent the corrected satellite coordinates in the EFEC system and the satellite coordinates calculated from the broadcast ephemeris, respectively; \mathbf{R} is the transformation matrix from the satellite-fixed coordinate system to the ECEF system [26,27]; r and \dot{r} represent the satellite position and velocity calculated from the broadcast ephemeris, respectively.

It should be indicated that the orbit products provided by IGS ACs in this article are with respect to the Center of Mass (CoM) of satellites. In contrast, the orbits of PPP-B2b products are with respect to the satellite Antenna Phase Center (APC); the BDS is based on the APC of B3I frequency, while GPS is based on the APC of IF combination [26]. Therefore, the antenna phase center correction should be considered. The relationship between APC and CoM can be described by,

$$\begin{bmatrix} X_{APC} \\ Y_{APC} \\ Z_{APC} \end{bmatrix} = \begin{bmatrix} X_{CoM} \\ Y_{CoM} \\ Z_{CoM} \end{bmatrix} + \mathbf{A}^T \cdot \begin{bmatrix} N_{PCO} \\ E_{PCO} \\ U_{PCO} \end{bmatrix} \quad (3)$$

where $[X_{APC} \ Y_{APC} \ Z_{APC}]^T$ and $[X_{CoM} \ Y_{CoM} \ Z_{CoM}]^T$ represent the APC and CoM satellite position in the EFEC system; $[N_{PCO} \ E_{PCO} \ U_{PCO}]^T$ represent the PCO correction of the satellite from the latest "igs14.atx" file released by IGS; \mathbf{A} is the satellite attitude matrix.

2.2. PPP-B2b Clock Recovery

The clock corrections broadcast by PPP-B2b can be recovered to form the precise clock by [26],

$$t^s = t_{brdc}^s - C_0/c \tag{4}$$

where t^s , t_{brdc}^s , C_0 , and c represent satellite precise clock, satellite clock calculated from the broadcast ephemeris, PPP-B2b clock corrections, and the speed of light in a vacuum, respectively.

It should be indicated that the BDS-3 precision clock provided by PPP-B2b is based on the B3I frequency, and all RTS clocks are based on the IF combination [26]. Therefore, all of these clocks for a GNSS system should be projected to one frequency. According to [26], the following method can be adopted to realize such projection,

$$t_j^s = t^s - b_j^s \tag{5}$$

where t_j^s is the satellite precise clock of signal j ; b_j^s represents the DCB between signal j and B3I.

2.3. Orbit and Clock Evaluation Methods

Several methods can be utilized to evaluate the accuracy of precise orbit and clock. For example, the overlapping orbit comparison, satellite laser ranging inspection, and comparison with a reference product. The first two usually are used to evaluate the final products of IGS precise products. Thus, the third method is adopted in this paper by using the final products provided by WHU as references. The orbit differences can be expressed as,

$$\begin{bmatrix} \Delta X \\ \Delta Y \\ \Delta Z \end{bmatrix}_t = \begin{bmatrix} X_{RT} \\ Y_{RT} \\ Z_{RT} \end{bmatrix}_t - \begin{bmatrix} X_{WHU} \\ Y_{WHU} \\ Z_{WHU} \end{bmatrix}_t \tag{6}$$

where t is the epoch number; $[\Delta X \ \Delta Y \ \Delta Z]^T$, $[X_{RT} \ Y_{RT} \ Z_{RT}]^T$, and $[X_{WHU} \ Y_{WHU} \ Z_{WHU}]^T$ are the orbit differences, real-time orbit, and final orbit vector.

The clock products from different ACs contain a benchmark inconsistency error. In this paper, to eliminate the system inconsistency, the GPS and BDS-3 constellations use G01 and C19 as reference satellites for the single difference from other satellites [28]. The STD of the clock difference between real-time and the reference clock after a single difference is estimated. The degree of clock consistency greatly influenced the solution accuracy of PPP [29]. The PPP-B2b products are estimated using the real-time observations collected by the regional tracking stations in China. Thus, the satellites rise or fall more frequently compared with using global observations. Furthermore, it is challenging to select a stable reference BDS satellite to generate the inter-satellite differences. To assess the accuracy of PPP-B2b clock products, we re-edited the inter-satellite difference clock using the method proposed by [23]. The expression of this method can be written as,

$$\nabla \Delta t^s = (t_{RT}^s - t_{WHU}^s) - \frac{1}{M} \sum_{i=1}^M (t_{RT}^i - t_{WHU}^i) \tag{7}$$

where $\nabla \Delta t^s$ is the double-difference clock value; t_{RT}^s is PPP-B2b real-time clock; t_{WHU}^s is the final precise clock of WHU; M is the number of available satellites.

Due to the observation discontinuity of the BDS satellites, the clock values estimated in Equation (7) are segmented, which affects the clock STD value. Therefore, the discontinuity is compensated by,

$$\nabla \Delta t_t^s = \nabla \Delta t_t^s - \Delta D_{t,t-1} \tag{8}$$

With

$$\Delta D_{t,t-1} = \begin{cases} \frac{1}{M} \sum_{i=0}^M \Delta \nabla \Delta t_{t,t-1}^i, \left| \frac{1}{M} \sum_{i=0}^M \Delta \nabla \Delta t_{t,t-1}^i \right| \geq 0.1 \text{ ns} \\ 0, \left| \frac{1}{M} \sum_{i=0}^M \Delta \nabla \Delta t_{t,t-1}^i \right| < 0.1 \text{ ns} \end{cases} \quad (9)$$

where $\Delta D_{t,t-1}$ is the compensation term to compensate the discontinuity in the double-difference clock; $\Delta \nabla \Delta t_{t,t-1}^i$ is the inter-epoch difference clock based on double difference clock.

2.4. Mathematical Model of Real-Time Single-/Dual-Frequency PPP

The measurements used for RT-PPP are pseudo-range (P) and carrier-phase (L), which can be expressed as [29,30],

$$P_j = \rho_r^s + c(t_r - t^s) + I_{r,j}^s + T_r^s + c(b_{r,j} - b_j^s) + \varepsilon_{P,j} \quad (10)$$

$$L_j = \rho_r^s + c(t_r - t^s) - I_{r,j}^s + T_r^s - \lambda_j(N_j + B_{r,j} - B_j^s) + \varepsilon_{L,j} \quad (11)$$

where ρ_r^s indicates the geometric distance from the satellite s to the receiver r ; t_r and t^s are the receiver clock and the satellite clock offset, respectively; $I_{r,j}^s$ and T_r^s are the ionospheric delay and tropospheric delay, respectively; $b_{r,j}$ and b_j^s are the DCB of the pseudo-range on receiver and satellite, respectively; λ_j and N_j are wavelength and ambiguity of carrier-phase; $B_{r,j}$ and B_j^s denote the Un-calibrated Phase Delay (UPD) on the satellite and receiver, respectively; $\varepsilon_{P,j}$ and $\varepsilon_{L,j}$ are observing noise of pseudo-range and carrier-phase, respectively.

2.4.1. Dual-Frequency PPP

The dual-frequency ionosphere-free combination pseudo-range and carrier-phase are used to form the observations of dual-frequency PPP [31],

$$P_{IF} = \frac{f_i^2}{f_i^2 - f_j^2} P_i - \frac{f_j^2}{f_i^2 - f_j^2} P_j = \rho_r^s + c(t_r - t^s) + T_r^s + \varepsilon_{P,IF} \quad (12)$$

$$L_{IF} = \frac{f_i^2}{f_i^2 - f_j^2} L_i - \frac{f_j^2}{f_i^2 - f_j^2} L_j = \rho_r^s + c(t_r - t^s) - \lambda_{IF} N_{IF} + T_r^s + \varepsilon_{P,IF} \quad (13)$$

where f_i is the frequency number; the other symbols have the same means as above.

In addition, if the observed frequencies in Equations (12) and (13) are different from that of precise real-time products, a DCB correction should be applied [32]. In this study, both B1I+B3I and B1I+B2b IF combinations are employed for static and kinematic PPP solutions, and the following equations should be employed,

$$\begin{cases} t_{B1I,B3I}^s = t^s - \frac{f_{B1I}^2}{f_{B1I}^2 - f_{B3I}^2} b_{B1I}^s \\ t_{B1I,B2b}^s = t^s - \left(\frac{f_{B1I}^2}{f_{B1I}^2 - f_{B2b}^2} b_{B1I}^s - \frac{f_{B2b}^2}{f_{B1I}^2 - f_{B2b}^2} b_{B2b}^s \right) \end{cases} \quad (14)$$

where $t_{B1I,B3I}^s$ and $t_{B1I,B2b}^s$ represent satellite precise clocks using the B1I+B3I and B1I+B2b IF combinations; f_{B1I} , f_{B2b} and f_{B3I} represent the frequencies corresponding to the B1I, B2b, and B3I observations, respectively.

In this case, the corresponding parameters that should be estimated are position vector, receiver clock offset, residual of troposphere delay, and IF ambiguity, which can be written as,

$$\mathbf{x} = [\delta x_r \quad \delta y_r \quad \delta z_r \quad c \cdot \delta t_r \quad d_{wet} \quad N_{IF}]^T \quad (15)$$

where δx_r , δy_r and δz_r indicate the corrected value of the receiver coordinates in three directions; δt_r and d_{wet} indicate the receiver clock offset and the zenith wet tropospheric delay; N_{IF} denotes the IF ambiguity vector.

2.4.2. Single-Frequency Model

For single-frequency PPP, Equations (10) and (11) form the observation equations. Here, the B1C and B2b measurements will be used in this paper. Thus, the satellite DCB corrections should be considered,

$$\begin{cases} t_{B1C}^s = t^s - b_{B1C}^s \\ t_{B2b}^s = t^s - b_{B2b}^s \end{cases} \quad (16)$$

Compared with the IF model, the ionospheric delay of each satellite and the receiver DCB cannot be eliminated. Therefore, they are estimated as parameters [33–35]. The corresponding state vector can be expressed as,

$$x = [\delta x_r \quad \delta y_r \quad \delta z_r \quad ct_r \quad d_{wet} \quad N_j \quad b_r \quad I_r] ^T \quad (17)$$

where b_r and I_r are the receiver DCB and the ionospheric delay vector.

Due to the correlations between the ionosphere and receiver DCB, we introduce the following pseudo-observations to improve the estimation accuracy of single-frequency PPP [33].

$$I_{r,j}^s = 40.28 STEC / f_j^2 + \omega_{I_{r,j}^s}, \omega_{I_{r,j}^s} \sim (0, \sigma_{I_{r,j}^s}^2) \quad (18)$$

where $STEC$ denotes the vertical electronic content obtained from the GIM model; $\sigma_{I_{r,j}^s}^2$ is the variance of the priori ionospheric model errors ($\omega_{I_{r,j}^s}$).

2.4.3. Parameter Modeling and Estimation

According to the observation functions and state parameters mentioned above, the sequential least square algorithm is adopted. The corresponding expressions can be described by,

$$V_k = A_k X_k - L_k \quad (19)$$

where V_k , A_k , X_k , and L_k denote the observation residual vector, the design coefficient matrix, the state vector, and the observation vector at time k , respectively.

Target function is,

$$V_k^T P_k V_k + V_{X,k}^T P_{X,k-1} V_{X,k} = \min \quad (20)$$

where $V_{X,k}$ denotes the difference between the current state vector X_k and its predicted vector \bar{X}_k ; $P_{X,k-1}$ denotes the weight matrix of the predicted state vector. The equation can be calculated by,

$$X_k = (A_k^T P_k A_k + P_{X,k-1})^{-1} (A_k^T P_k L_k + P_{X,k-1} \bar{X}_k) \quad (21)$$

$$P_{X,k}^{-1} = (A_k^T P_k A_k + P_{X,k-1})^{-1} \quad (22)$$

The corresponding posterior covariance matrix of the state vector

$$D_{X,k-1} = P_{X,k-1}^{-1} (V_k^T P_k V_k + V_{X,k}^T P_{X,k-1} V_{X,k}) / (n - m) \quad (23)$$

where n and m represent the number of satellites obtained at k and $k - 1$ epochs, respectively.

3. Experiments and Discussions

In this section, we collected four-day data to compare the accuracies of PPP-B2b orbit and clock to those of IGS RTS products. The positioning accuracies of PPP-B2b on dual-frequencies and single-frequency PPP are further studied with static and dynamic tests.

3.1. Static Data Collection

The real-time orbit and clock SSR products of PPP-B2b, CAS, DLR, GFZ, and WHU, the ultra-rapid products from WHU, and the broadcast ephemeris during the Days of Year (DOY) 354–357 in 2021 were collected. The distribution of the stations is illustrated in Figure 1. The IGS real-time SSR corrections were collected from the internet via the open-source software BNC Ver2.12.17 [36]. The static data from four MGEX stations (URUM, ULAB, WHU2, and JFNG) during DOYs of 354–357 of 2021 were collected.

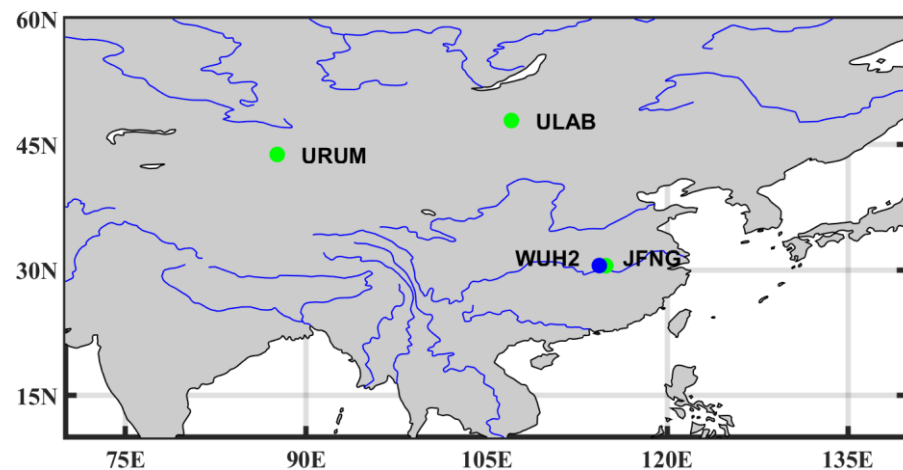


Figure 1. The location of 4 selected MGEX stations.

In the data analysis phase, (1) all of these orbit and clock products were projected to the same coordinate system and time system; (2) static test data were processed daily with dual-frequency IF PPP (B1I+B3I and L1+L2) and single-frequency PPP (B1C and L1); (3) the corresponding GPS data were also processed as a comparison; (4) the reference coordinates obtained from the MGEX weekly SINEX file. The details of the static data processing strategies are listed in Table 3. It is worth noting that the B1C observation is BDS-3 new signal, which is not used for orbit determination and clock calculation. Thus, the corresponding DCB correction should be applied to the observations.

Table 3. PPP processing strategies of static test.

Item	Processing Strategies
GNSS	BDS-3 and GPS
Signal selection of IF PPP	BDS-3: B1I+B3I GPS: L1+L2
Signal selection of SF PPP	BDS-3: B1C GPS: L1
Interval	30 s
Cutoff angle	10°
Weight method	Elevation angle dependent
Troposphere	Estimate the wet component
Ionospheric	IF PPP: IF combination SF PPP: Estimated
PCO/PCV	IGS14.atx
Ambiguity	Estimated
Adjustment	Sequential least square
Satellite DCB	Corrected by DCB products
Receiver DCB	IF PPP: IF combination SF PPP: Estimated

The available satellites and PDOP are the two critical indexes for positioning accuracy analysis; therefore, the number of visible satellites and the PDOP values for both BDS-3

and GPS are presented in Figure 2. The number of available BDS-3 satellites on average are 8.4, 8.1, 7.8, and 8.1, with the corresponding PDOP of 2.1, 2.2, 2.9, and 2.3 for JFNG, ULAB, URUM, and WUH2 stations. For GPS, the average number of available satellites are 6.8, 7.1, 6.8, and 6.6, with the corresponding PDOP of 2.5, 2.6, 2.9, and 2.7 for JFNG, ULAB, URUM, and WUH2 stations.

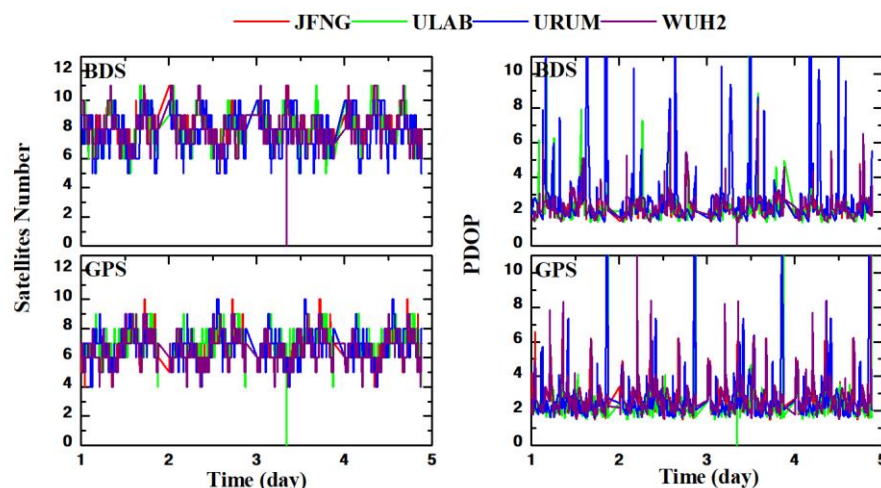


Figure 2. Number of visible satellites and PDOP values of the four MEGX stations.

3.2. Assessments of BDS-3 Real-Time Orbits and Clock Products

To evaluate the accuracies of PPP-B2b BDS-3 real-time orbits and clocks from CAS, DLR, GFZ, and WHU, as well as the broadcast ephemeris objectively, this study uses the final precision product from WHU as the reference. The B2b corrected GPS orbit and clock are also studied as a comparison. The time series of the orbit errors in radial, along-track, and cross-track directions, as well as the clock errors, are depicted in Figure 3. The corresponding statistics in terms of RMSE and STD are shown in Figures 4 and 5. In Figure 3, the orbit errors of different real-time products of BDS are within 20 cm, 60 cm, and 60 cm in radial, along-track, and cross-track directions. The BDS B2b corrected and broadcast orbit error in radial and along-track directions are similar to those of other real-time products; in the cross-track direction, however, the fluctuations of B2b-corrected and BDS broadcast orbit errors are more significant than those of other real-time products. The B2b corrected GPS orbit error is similar to that of the B2b corrected BDS orbit. As plotted in Figure 4, the statistic orbit accuracies of the IGSO satellites, C38~C40, are much lower than those of MEO satellites, especially while using the SSR corrections from GFZ. Generally, the orbit RMSE values of the real-time products from CAS, DLR, GFZ, WHU, and WHU_U (ultra-precise products) are within 10 cm in the radial, along-track, and cross-track components for MEO satellites. The RMSE of BRDC, PPP-B2b for BDS-3, are about 20 cm in the radial component and 50 cm in the along-track and cross-track components; the B2b corrected orbit for GPS has a similar performance as those for BDS in three directions. According to earlier studies, the higher accuracy in the radial direction is related to the high-quality satellite hydrogen and rubidium clocks [37]. In Figure 3, it is noted that systematic biases existed among different real-time clock products, especially the B2b corrected BDS and GPS clocks. This systematic clock bias is caused by pseudorange observation and can be absorbed by ambiguities [24,38]. In Figure 5, The clock STD of the real-time products from CAS, DLR, GFZ, WHU, and WHU_U are within 0.4 ns for BDS MEO satellites. In contrast, the STD of PPP-B2b is within 0.2 ns, and the STD of BRDC is within 1.0 ns. The STD of the B2b corrected GPS clock is 0.3 ns.

The average accuracies of real-time orbit and clock products are shown in Table 4. DLR did not provide SSR corrections for the three IGSO satellites, C38, C39, and C40, during this test; thus, the average accuracies of these three satellites are not considered. According to Table 4, the BDS-3 orbit accuracy in the radial component is higher than those in the along-

track and cross-track components. The RMSE of the BDS-3 PPP-B2b orbits in the radial, along-track, and cross-track components are 9.42 cm, 21.26 cm, and 28.65 cm, respectively. The accuracy of BDS-3 PPP-B2b orbits in terms of RMSE is lower than that of IGS centers products due to the distribution and number of the monitoring stations. Compared to the broadcast orbit, the IGS real-time products provide about 30.62~54.95% improvements in the radial component, and the improvement provided by BDS PPP-B2b is 2.89%. The STD of PPP-B2b clocks is 0.18 ns, which has the highest accuracy among these real-time products of BDS-3. The improvements of the BDS-3 real-time clock provided by PPP-B2b is 79.87% compared to broadcast ephemeris. For the GPS correction, the B2b corrected orbit RMSE in radial, along-track, and cross-track directions are 13.73 cm, 23.83 cm, and 17.96 cm, respectively, and the clock STD is 0.25 ns. For the user side, the positioning accuracy is mainly affected by the orbit in radial and the clock. Therefore, the PPP-B2b SSR products theoretically can provide precise positioning solutions.

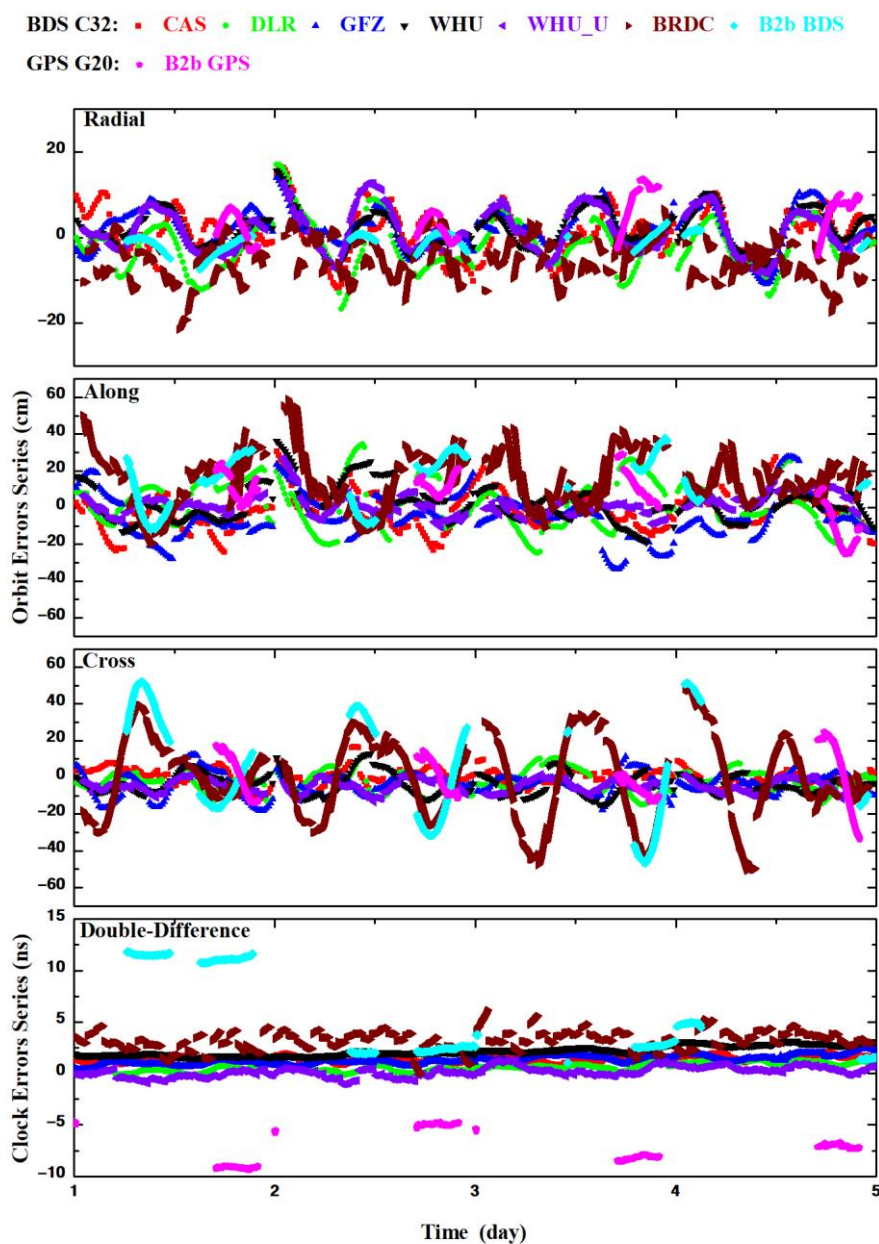


Figure 3. Time series of the orbit radial and clock errors of C32 and G20.

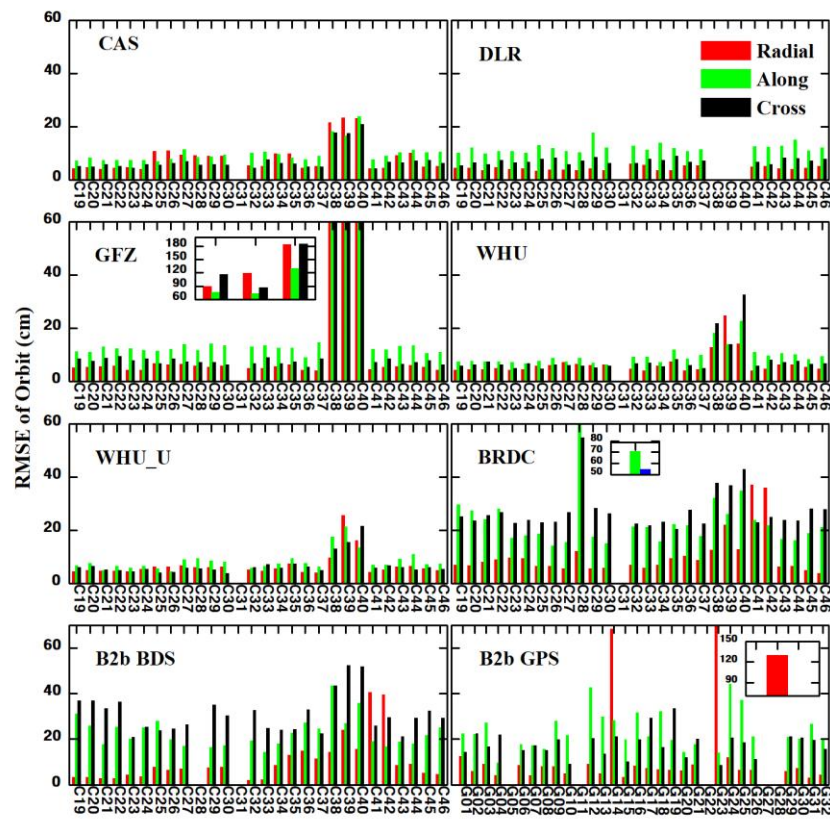


Figure 4. RMS of real-time orbit errors.

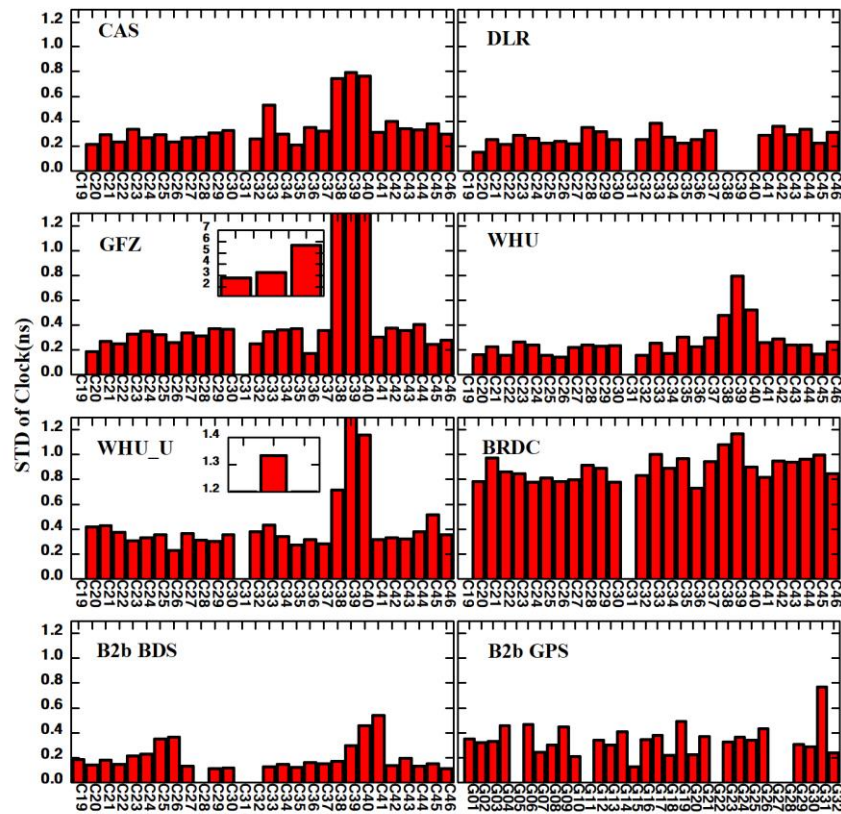


Figure 5. STD of real-time orbit clock errors.

Table 4. The average accuracies of real-time orbit and clock products.

Products	Orbit (cm)			Clock (ns)
	Radial	Along-Track	Cross-Track	
CAS	6.73	8.82	5.79	0.31
DLR	4.37	11.95	7.08	0.27
GFZ	5.41	12.40	7.63	0.31
WHU	5.38	8.57	6.41	0.22
WHU_U	5.39	7.25	5.54	0.35
BRDC	9.70	22.21	25.74	0.87
B2b BDS	9.42	21.26	28.65	0.18
B2b GPS	13.73	23.83	17.96	0.25

3.3. Accuracy and Convergence of RT-PPP in MEGX Stations

3.3.1. Dual-Frequency PPP

The time series of the position differences between the B1I+B3I PPP solutions of the four MEGX stations and the SINEX solutions on the E, N, and U components are presented in Figure 6. The average RMSE of the static PPP at JFNG, ULAB, URAM, and WUH2 stations is shown in Figure 7. Accordingly, the positioning accuracy of BDS-3 dual-frequency PPP based on the PPP-B2b real-time products is within 4.6 cm in the three directions for the four stations. In contrast, the GPS dual-frequency PPP with B2b correction is about 5.3 cm in three directions. The lower accuracy of GPS PPP with B2b corrections is caused by the product accuracy of GPS orbits and clocks, which has been studied in the above section. Additionally, the positioning accuracy of PPP-B2b-based positioning in the N component is higher than in the E component, which is related to the satellite's observation geometry strength of the carrier phase ambiguity. Most BDS-3 satellites have a north-south ground track and, thus, provide strong observation geometry strength in N directions and better positioning accuracy. In addition, the fixing ambiguity may improve the positioning accuracy in the E components [39], and similar results can be obtained in [22,40]. In general, the positioning accuracy of static RT-PPP with PPP-B2b is slightly lower than that of IGS real-time products, but higher than that of WHU ultra-rapid products and broadcast ephemeris.

The statistics accuracy in terms of RMSE of static B1I+B3I PPP using different real-time products is listed in Table 5. The positioning accuracies of BDS-3 PPP with PPP-B2b service are 4.8 cm and 5.4 cm in horizontal and 3D components, respectively. While using GPS, the positioning accuracy is slightly lower than that of BDS-3, with 5.4 cm and 5.9 cm in horizontal and 3D components, respectively. This demonstrates that the PPP-B2b service has the capability of providing centimeter-level positioning accuracy for users in China and neighboring countries while using the dual-frequency static PPP mode. However, the accuracy of PPP using PPP-B2B services is still lower than those solutions based on IGS real-time products. Among these solutions, the solution based on the products of WHU has the highest accuracy in horizontal components with 1.1 cm. In comparison, the solution based on the CAS products has the highest accuracy in 3D with 1.9 cm. The solutions based on DLR real-time products present the worst accuracy with 3.5 cm and 3.9 cm in horizontal and 3D components, respectively. Additionally, the horizontal and 3D positioning accuracies using WHU ultra-rapid products are 10.5 cm and 12.1 cm, respectively, while those based on broadcast ephemeris are 23.9 cm and 27.7 cm. Generally, the B1I+B3I BDS-3 PPP based on PPP-B2b SSR corrections can provide users with centimeter-level static positioning solutions, which is close to these based on IGS RTS SSR corrections, especially in horizontal components.

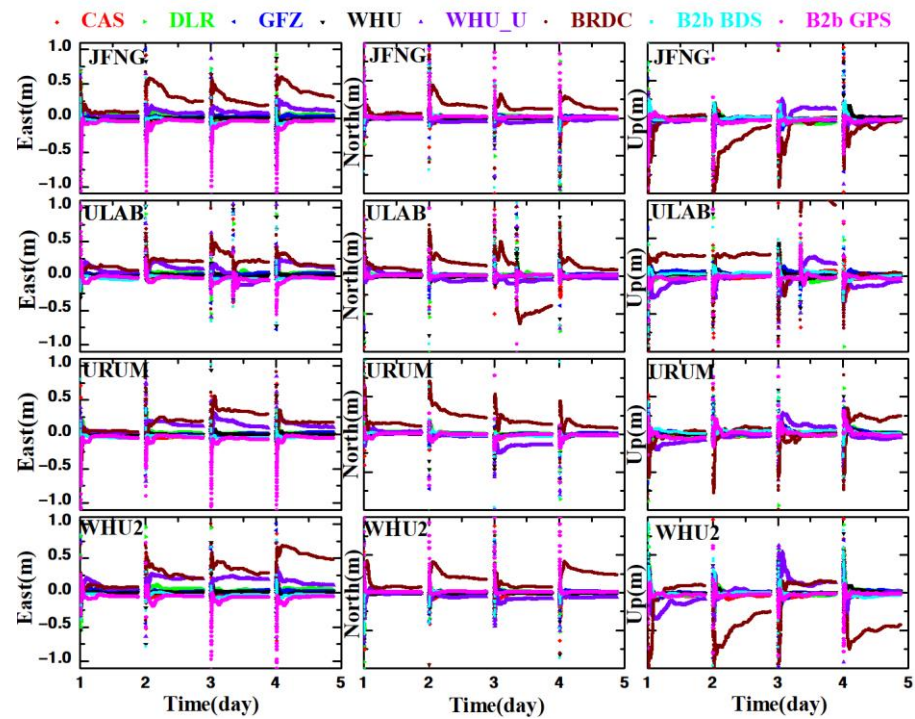


Figure 6. Error series of the four-day IF static PPP solution.

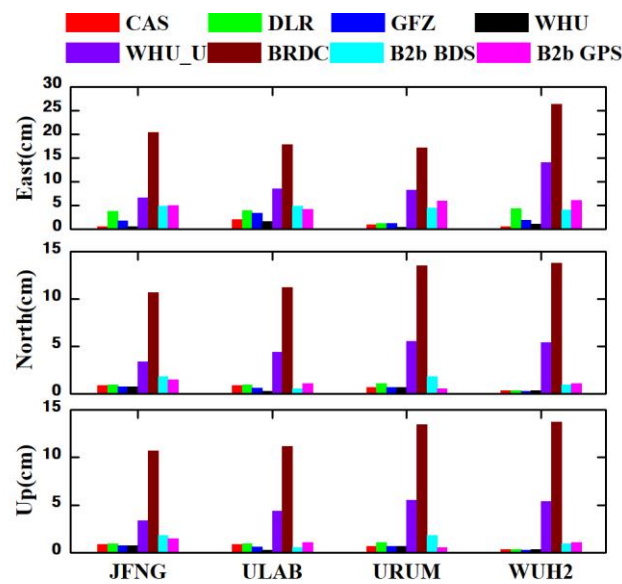


Figure 7. The average accuracy of the four-day IF static PPP solution.

Table 5. Average dual-frequency PPP positioning accuracy of the four MGEX stations (unit: cm).

Direction	CAS	DLR	GFZ	WHU	WHU_U	BRDC	B2b BDS	B2b GPS
E	1.1	3.3	2.1	0.9	9.4	20.4	4.6	5.3
N	0.7	0.8	0.6	0.5	4.7	12.3	1.2	1.0
U	1.4	1.8	1.4	1.8	6.0	13.2	2.4	2.2
2D	1.3	3.5	2.2	1.1	10.5	23.9	4.8	5.4
3D	1.9	3.9	2.7	2.1	12.1	27.7	5.4	5.9

Convergence time is another crucial index for PPP evaluation. In this paper, we define the convergence criteria of static PPP to be that the position accuracies in horizontal and

vertical are continuously better than 10 cm and 20 cm for at least 10 min. The convergence times of static PPP for each MGEX station are presented in Figure 8. Since it is difficult to converge while using WHU ultra-rapid product and broadcast ephemeris, we only provide the convergence times of PPP using IGS real-time products and PPP-B2b products. As shown in Figure 8, the convergence times of BDS-3 PPP based on PPP-B2b products are within 15 min. The PPP-B2b-based GPS PPP presents the slowest convergence time, with an average convergence time of 52 min and the longest time of 109 min. The reason for the longer convergence time of JFNG may be caused by the inconsistency of the satellites' orbit errors, as shown in Figure 4, in which the fluctuations of B2b corrected orbit is more significant than that of B2b corrected BDS.

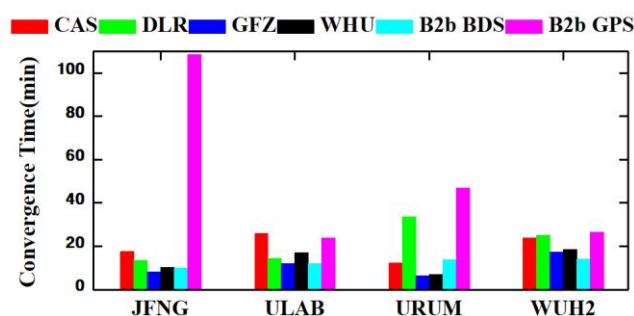


Figure 8. Convergence time of static dual-frequency PPP using different real-time orbit and clock products.

3.3.2. Single-Frequency PPP

In this section, a single-frequency PPP model with ionospheric and receiver DCB constraints is used. The time series of position differences between the static single-frequency PPP and the reference results in the E, N, and U for each station are shown in Figure 9, and the corresponding statistics are presented in Figure 10. The positioning accuracy in terms of RMSE of BDS B1C PPP with PPP-B2b SSR products is better than 5.5 cm in the E, N, and U for each station. While using GPS L1, the PPP accuracy is better than 5.6 cm in three components. The positioning accuracy of single-frequency PPP with PPP-B2b is comparable to that of IGS real-time RTS products, which have similar performance to the dual-frequency PPP. The positioning accuracy of static single-frequency PPP using WHU ultra-rapid product and broadcast ephemeris is much lower than that with PPP-B2b. The maximum positioning error for broadcast ephemeris-based solution exceeds 39.5 cm in the three components.

According to the statistics of average positioning error in Table 6, single-frequency RT-PPP based on PPP-B2b SSR products and IGS RTS SSR products (except DLR) can satisfy the demand for centimeter-level high-precision real-time positioning accuracy. While using PPP-B2b SSR products, the position accuracies in horizontal and 3D of B1C PPP are 5.4 cm and 7.7 cm, respectively. While using the IGS RTS products, the B1C PPP based on WHU products provides the highest accuracy within 3.5 cm in horizontal, and the PPP based on GFZ products provides the highest accuracy in 3D with 7.0 cm among evaluated the IGS RTS products. In contrast, the DLR real-time products provide the worst static B1C PPP positioning accuracy with 5.5 cm and 14.3 cm in the horizontal and 3D. The horizontal/3D positioning accuracies using WHU ultra-rapid products and broadcast ephemeris were about 7.6/13.1 cm and 18.3/43.5 cm, respectively, much lower than those of PPP-B2b PPP. As a comparison, the positioning accuracies of GPS L1 PPP based on PPP B2b SSR products are 5.4 cm and 7.8 cm, similar to those of BDS-3 B1C PPP.

To present the convergence speed of single-frequency B1C PPP, we redefine the convergence criteria of static PPP to be that the position accuracies in horizontal and vertical are continuously better than 20 cm and 40 cm for at least 10 min. The convergence times of static single-frequency PPP based on different SSR products for each MGEX station are shown in Figure 11, in which the average convergence times of BDS-3 B1C PPP and GPS L1 PPP using PPP-B2b SSR products are 80 min and 73 min, respectively. For solutions

based on the four IGS real-time products, the converge times with CAS's products are the shortest among other products, with an average time of 65 min. The DLR products-based solutions converge the slowest with an average time of 95 min.

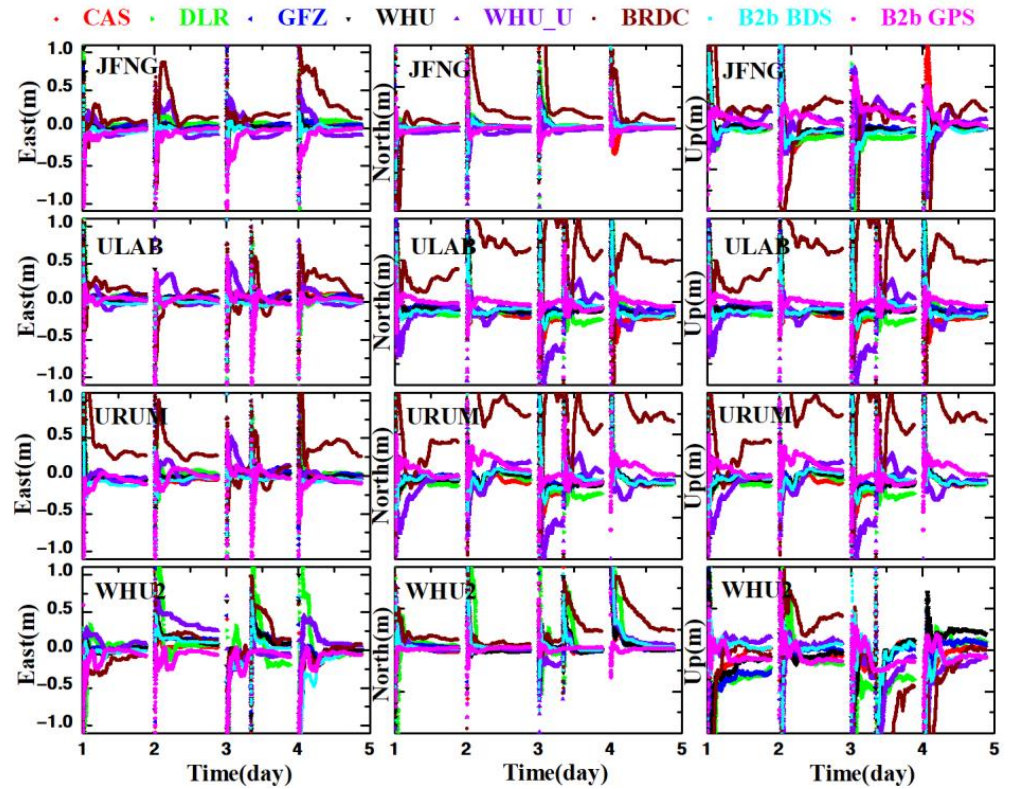


Figure 9. Time series of position errors of the four-day single-frequency static PPP.

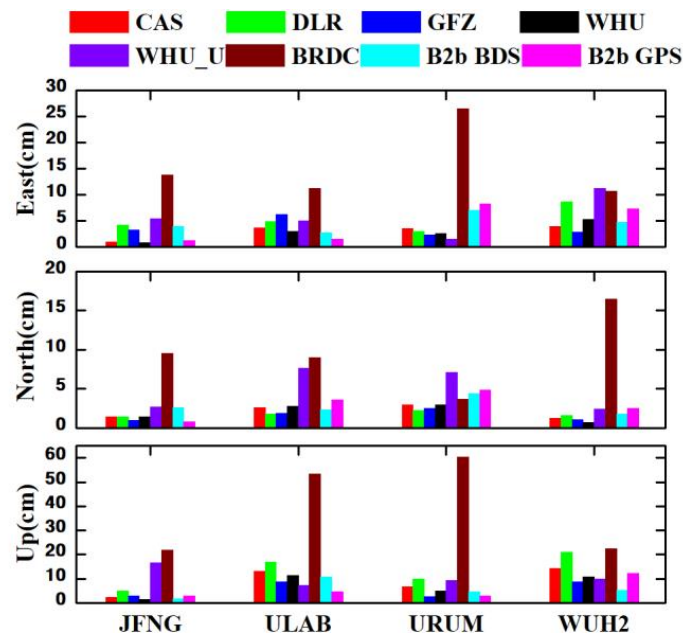
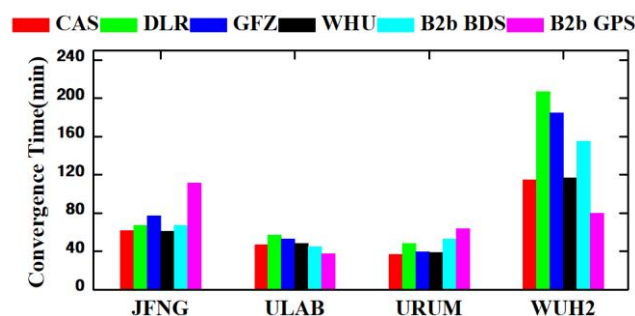


Figure 10. Average accuracy of the four-day single-frequency static PPP.

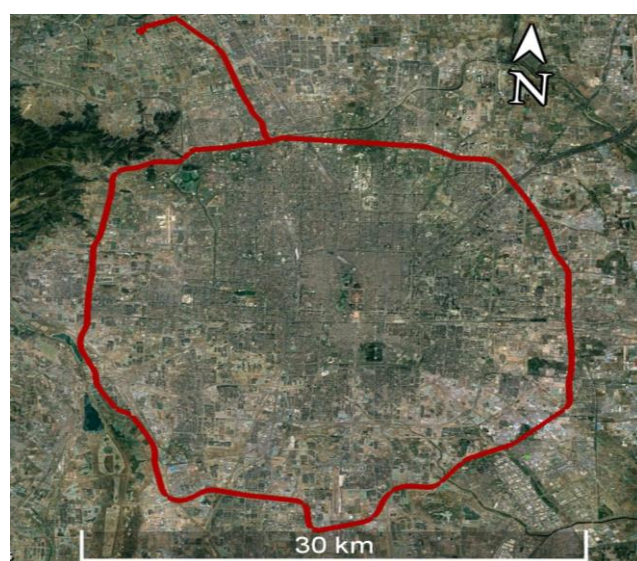
Table 6. The average positioning accuracy at the four stations (unit: cm).

Direction	CAS	DLR	GFZ	WHU	WHU_U	BRDC	B2b BDS	B2b GPS
E	3.0	5.2	3.7	2.9	5.8	15.5	4.6	4.6
N	2.0	1.8	1.6	2.0	4.9	9.7	2.8	2.9
U	9.1	13.2	5.7	7.0	10.7	39.5	5.5	5.6
2D	3.6	5.5	4.0	3.5	7.6	18.3	5.4	5.4
3D	9.8	14.3	7.0	7.8	13.1	43.5	7.7	7.8

**Figure 11.** Convergence time of single-frequency PPP using different SSR products.

3.4. Accuracy of Real-Time Vehicle-Borne PPP

The dynamic test is carried out on DOY 357 in 2021 from 06:00 to 08:30 on the fifth ring road with Inertial Navigation System (INS) (NovAtel SPAN EPSON G370) and NovAtel GNSS receiver, which receives the B1I and B2b signal from BDS-3, and L1 and L2 signal from GPS. To study the PPP-B2b performance in complex environments, especially the performance of new signal B2b, we equipped a GNSS jammer to interfere with the received GNSS signals. The jammer reduces the number of visible satellites rather than affecting the observed distances. In the dynamic test, the vehicle drove about 40 km in the north–south direction and 30 km in the east–west direction. The tight integration of GPS+BDS RTK and INS provided by Inertial Explorer software were used as reference values for the dynamic test, and the corresponding trajectory is presented in Figure 12.

**Figure 12.** The trajectory of vehicle dynamic test.

The positioning strategies are listed in Table 7. It should be noted that the satellite DCB products from both real-time SSR and IGS final products do not contain the satellite

DCB value of C7D (B2b). Therefore, the DCB value of C7Z from CAS' was used to weaken the influence of satellite DCB on B2b frequency with ignoring the intra-frequency error. The number of visible satellites and corresponding PDOP values are presented in Figure 13. The average number of visible BDS-3 and GPS satellites during the 4-h dynamic test in Beijing are 8.9 and 2.0, respectively, and the average corresponding PDOP value of BDS-3 and GPS are 6.3 and 2.4, respectively. The sharp changes in the number of visible satellites are affected by the equipped GNSS jammer and further affect the PDOP values.

Table 7. PPP processing strategies of dynamic test.

Item	Processing Strategies
GNSS	BDS-3 and GPS
Signal selection of IF PPP	B1I+B2b GPS: L1+L2
Signal selection of SF PPP	BDS-3: B2b GPS: L1
Interval	1 s
Cutoff angle	10°
Weight method	Elevation angle dependent
Troposphere	Estimate the wet component
Ionospheric	IF PPP: IF combination SF PPP: Estimated
PCO/PCV	IGS14.atx
Ambiguity	Estimated
Adjustment	Sequential least square
Satellite DCB	Corrected by DCB products
Receiver DCB	IF PPP: IF combination SF PPP: Estimated

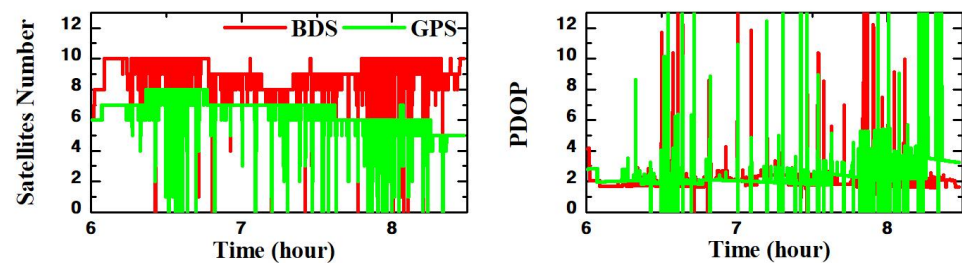


Figure 13. Number of visible satellites and PDOP values during the dynamic test.

Figure 14 presents the time series of position errors of vehicle-borne dual-frequencies (B1i+B2b and L1+L2) PPP, single frequency PPP (L1 and B2b) by comparing with the RTK/INS tight integration solutions in E, N, and U components. It is noted that the large fluctuations in the three components occur in dual-frequencies and single frequencies PPP, especially in the U components. Comparing to the visible satellite number presented in Figure 13, the presence of significant error components coincided with epochs of poor observations, which results in positioning discontinuity and further leads to PPP re-convergence. We chose dual-frequency PPP during epochs 3587 to 3588, red box in Figure 14, to further analyze the effect of GNSS signal blockage. At the period of epochs 3587 and 3588, the visible satellite is 0, and the BDS cannot provide continuous positioning results. At epoch 3589, the number of visible satellites is 8, and the positioning error at E, N, and U components are 4 m, −2 m, and −4 m, respectively. The average visible satellite number during epochs 3589 and 3900 is 8.9, and the B1I+B2b combination PPP with PPP-B2b converged to 0.5 and 1.0 m positioning accuracy in both horizontal and vertical components. The convergence time is 85 s in this period, and the average PDOP value is 2.2. The error components of single frequency PPP, L1 and B2b, present similar statuses.

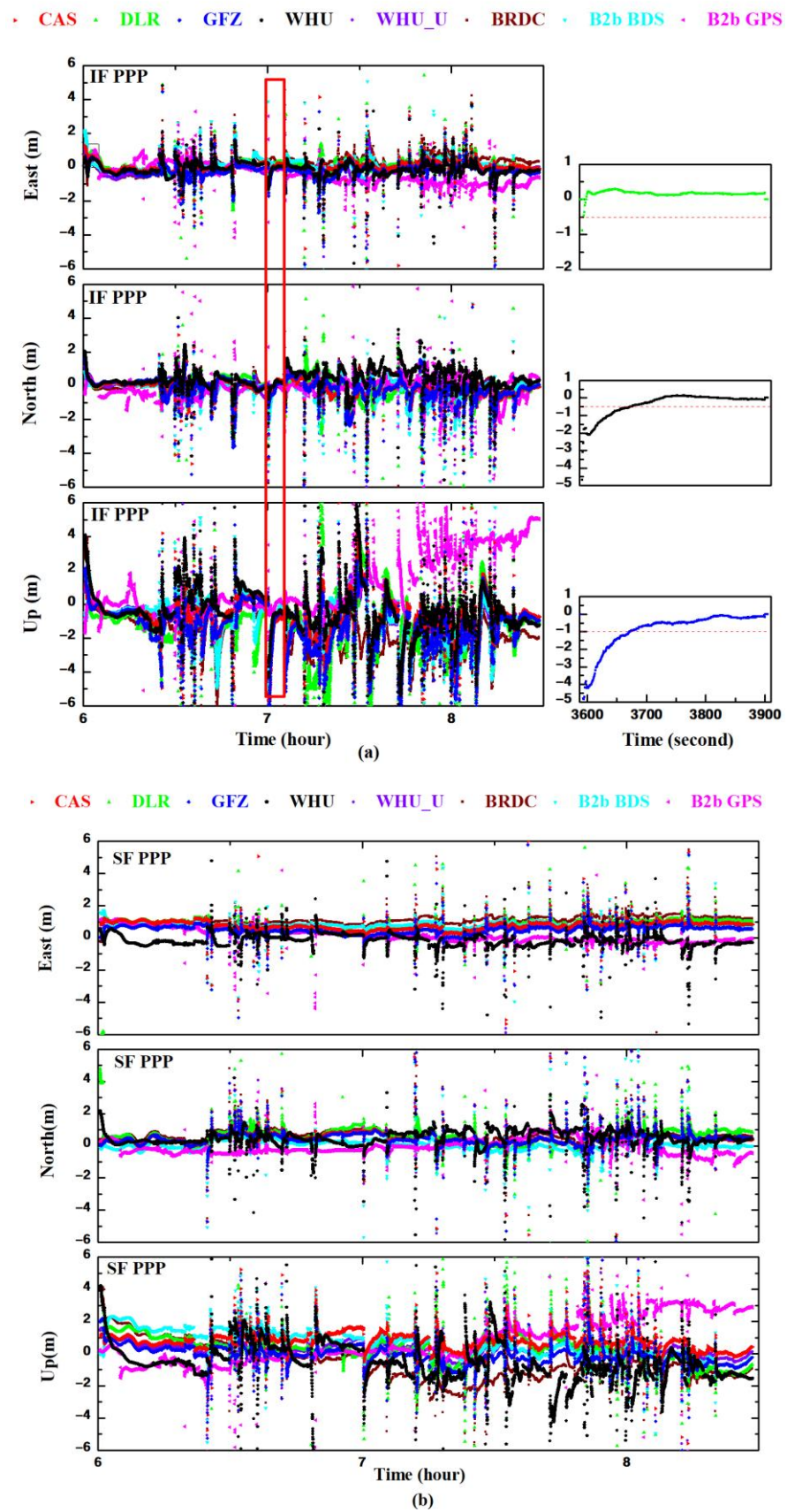


Figure 14. Time series of position errors of the dual-(a)/single (b)-frequency vehicle-borne RT-PPP using different SSR products.

The accuracies in terms of RMSE of vehicle-borne dual-frequency PPP and single-frequency PPP based on different SSR products are shown in Tables 8 and 9. For the dual-frequency PPP, the positioning accuracy of the BDS-3 B1I+B2b PPP using PPP-B2b SSR products is 35.8 cm, 55.0 cm, and 121.3 cm in the E, N, and U components, respectively. In contrast, the B1I+B2b PPP positioning accuracy using CAS products is the highest in horizontal with 58.9 cm, and WHU products are the highest in 3D with 129.7 cm. The solutions based on broadcast ephemeris (67.5 cm and 182.4 cm in horizontal and 3D components) have the worst positioning accuracy among the seven products. The GPS L1+L2 PPP is 57.0 cm, 47.9 cm, and 101.4 cm in the E, N, and U components. The GPS L1+L2 PPP solution has the highest 3D accuracy (126.0 cm) and the worst horizontal accuracy (74.5 cm) compared to the BDS-3 B1I+B2b PPP using the SSR product of both PPP-B2b and IGS RTS.

Table 8. Position RMSE of vehicle-borne real-time dual-frequency PPP using different SSR products (unit: cm).

Direction	CAS	DLR	GFZ	WHU	WHU_U	BRDC	B2b BDS	B2b GPS
E	27.8	33.0	35.4	34.9	35.5	49.2	35.8	57.0
N	61.9	51.8	53.9	62.1	49.7	46.1	55.0	47.9
U	115.7	139.4	138.2	108.4	125.5	169.4	121.3	101.4
2D	58.9	61.4	64.5	71.2	61.1	67.5	65.7	74.5
3D	129.9	152.3	152.5	129.7	139.5	182.4	137.9	126.0

Table 9. Position RMSE of vehicle-borne real-time single-frequency PPP using different SSR products (unit: cm).

Direction	CAS	DLR	GFZ	WHU	WHU_U	BRDC	B2b BDS	B2b GPS
E	80.0	88.6	54.3	79.4	73.9	111.8	87.1	42.3
N	53.9	72.0	53.1	156.7	57.3	72.7	32.9	47.8
U	88.6	87.8	60.0	178.6	57.3	126.3	103.5	129.2
2D	96.5	114.2	75.9	175.7	93.5	133.4	93.1	63.9
3D	131.0	144.0	96.8	250.5	109.6	183.7	139.2	144.1

For the single-frequency PPP, the positioning accuracy of B2b frequency PPP based on PPP-B2b products in E, N, and U components are 87.1 cm, 32.9 cm, and 103.5 cm, respectively; those positioning accuracies of GPS L1 PPP are 42.3 cm, 47.8 cm, and 63.9 cm, respectively. While using GPS, the positioning accuracy is slightly higher in horizontal components (42.3 cm and 47.8 cm) but much worse in the U direction (129.2 cm). For the solutions based on IGS RTS real-time products, the positioning accuracy using GFZ real-time products is the best, with 75.9 cm and 96.8 cm in horizontal and 3D components, respectively. The positioning accuracy with WHU real-time products is 175.7 cm and 250.5 cm in horizontal and 3D components, respectively, which are the worst among other real-time products. In Figure 14, a noticeable systematic error exists in the N and U components, which are caused by the unabsorbed satellite clock errors. Compared to BDS-3 B1I+B2b PPP, the BDS-3 B2b PPP provides smoother position solutions, especially after satellites signal re-tracking, which is caused by the greater noise of the dual-frequency IF and high-accuracy of prior ionosphere data used in single-frequency PPP.

Figure 15 shows the radial, along-track, and cross-track RMS values of the orbit's errors and clock STD values for each type of real-time product, as well as the positioning accuracy of static and dynamic with single/dual-frequency PPP. In static PPP, the IGS real-time product positioning accuracy is better than that of PPP-B2b, and BRDC positioning accuracy is the worst among the seven products. This is consistent with the orbit and clock accuracies of each real-time product. In dynamic PPP, affected by the complex positioning environment, the positioning accuracy of various products is similar.

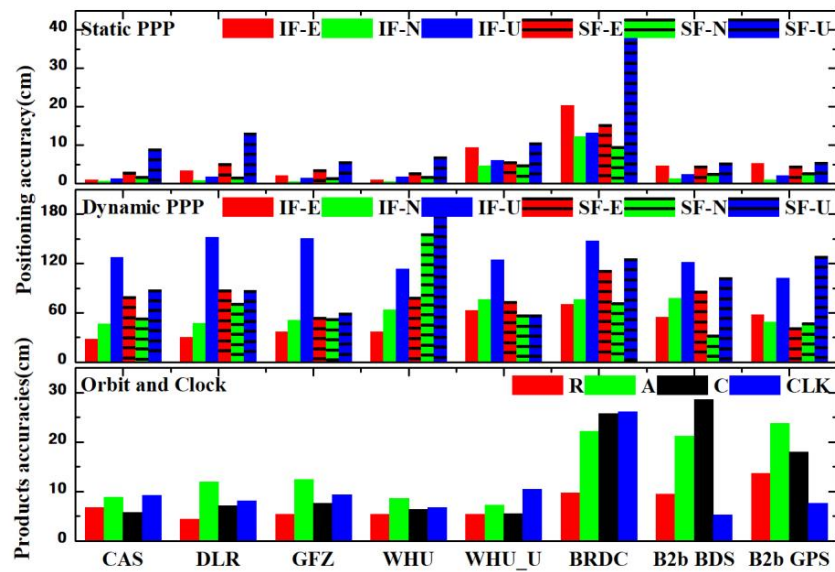


Figure 15. The average accuracy of positioning and real-time products.

It also can be found from Figure 15 that the accuracies of the real-time WHU orbits and clock products are similar to other ACs, but the positioning of single frequency PPP with WHU products is lower than that of other ACs. This is because the WHU BDS real-time clock products contain systematic errors. The RMSE of different BDS real-time clock products with respect to the WHU final clock product is presented in Figure 16. It can be clearly found that the RMSE value of WHU BDS real-time products is more significant than that of other products.

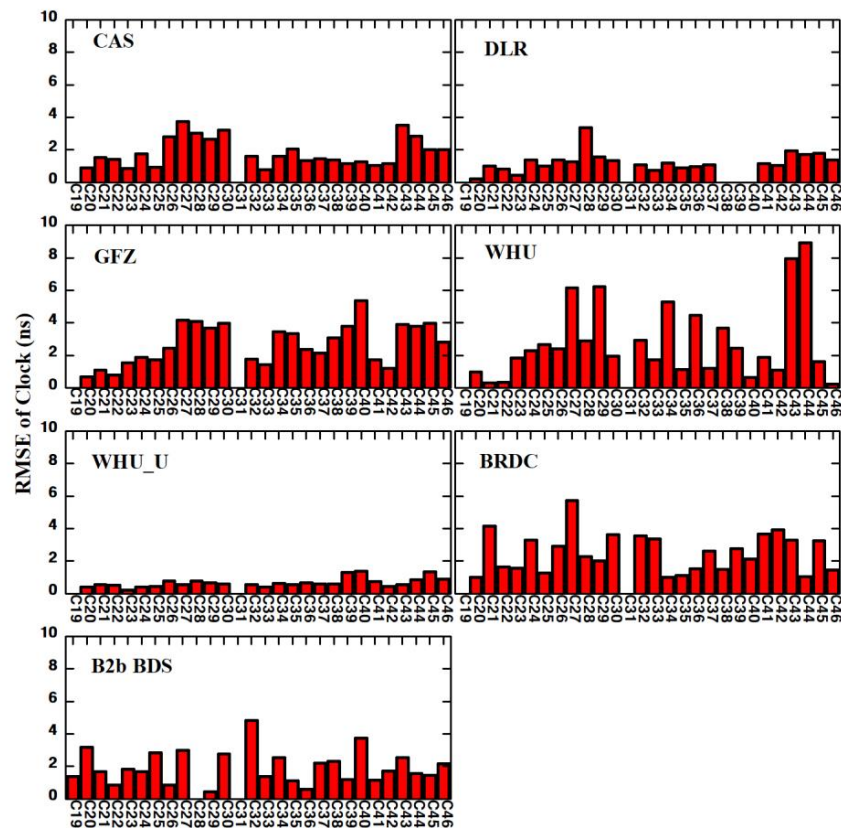


Figure 16. The RMSE of real-time orbit clock errors.

4. Conclusions

Real-time orbits and clocks are crucial factors for RT-PPP applications. To evaluate the impacts of existing real-time orbit and clock products (BDS-3 PPP-Bb and IGS RTS), this study provides comprehensive assessments of the accuracy of these real-time products and their influences on the positioning accuracy and convergence time of RT-PPP in both static and dynamic tests. After the descriptions of the evaluation methods for real-time orbits and clocks as well as the real-time single-/dual-frequency PPP models, BDS-3 new signals observations of B1C and B2b from the four MEGX stations and a set of the vehicle-borne test were used to find the conclusions of the assessment. The main conclusions can be summarized as follows.

For these real-time SSR products, the orbit accuracy of PPP-B2b SSR products is lower than these of IGS real-time products (CAS, DLR, GFZ, and WHU). However, the clock accuracy of PPP-B2b is better than these of IGS real-time products. Additionally, the accuracy of the real-time orbit and clock of BDS-3 provided by PPP-B2b is higher than that of GPS.

For real-time dual-frequency PPP, the position RMSEs of the four MEGX stations based on PPP-B2b SSR products are slightly lower than those based on the IGS RTS SSR products. Meanwhile, the BDS-3 B1I+B3I PPP positioning accuracy using the PPP-B2b service is centimeter-level which is better than that of GPS L1+L2 PPP. The dual-frequency B1I+B2b PPP positioning accuracy in the vehicle-borne test achieved submeter-level and meter-level in horizontal and vertical components in our test environment.

For the single-frequency RT-PPP based on PPP-B2b SSR products, the BDS-3 B1C PPP is lower than that of B1I+B3I PPP, providing about 10–20 cm-level positioning accuracy with MEGX data. While using the vehicle-borne B2b frequency data, the accuracy of BDS-3 PPP is very close to that of B1I+B2b PPP with submeter-level and meter-level in horizontal and vertical components.

In general, our work shows that both the BDS-3 PPP-B2b service and the IGS RTS can satisfy the demand for high-accuracy positioning in real time. However, these real-time products provided by IGS RTS are calculated from the global-distributed stations, which are more accurate than BDS-3 PPP-B2b, especially for GPS. However, IGS RTS are limited by the connection of the internet. Additionally, BDS-3 PPP-B2b introduces inter-satellite link technology and broadcasts SSR information by navigation signal, which gives it more significant potential in real-time precise positioning applications in the future.

Author Contributions: Conceptualization, C.Y., Y.Z. and Z.G.; Data curation, Q.X.; Funding acquisition, C.Y. and Z.G.; Investigation, R.L., C.Y. and Z.G.; Software, R.L.; Supervision, C.Y. and Z.G.; Visualization, R.L., Q.X. and J.L.; Writing—original draft, R.L.; Writing—review and editing, R.L., C.Y., Y.Z. and Z.G. All authors have read and agreed to the published version of the manuscript.

Funding: This research was partly supported by the National Key Research and Development Program of China (Grant No. 2020YFB0505802), the National Natural Science Foundation of China (NSFC) (Grants No. 42274022, No. 42274024).

Data Availability Statement: The datasets analyzed in this study are managed by the School of Land Science and Geomatics, China University of Geosciences, Beijing, and can be available on request from the corresponding author.

Acknowledgments: Thanks to the original observations provided by MEGX and the multi-system SSR products provided by the analysis centers CAS, DLR, GFZ, and WHU.

Conflicts of Interest: The authors declare no conflict of interest.

References

1. Yang, Y.; Gao, W.; Guo, S.; Mao, Y.; Yang, Y. Introduction to BeiDou-3 navigation satellite system. *Navigation* **2019**, *66*, 7–18. [[CrossRef](#)]
2. Yang, Y. Resilient PNT concept frame. *Acta Geod. Cartogr. Sin.* **2018**, *47*, 893.
3. Yang, Y.; Mao, Y.; Sun, B. Basic performance and future developments of BeiDou global navigation satellite system. *Satell. Navig.* **2020**, *1*, 1. [[CrossRef](#)]

4. Zumberge, J.; Heflin, M.; Jefferson, D.; Watkins, M.; Webb, F. Precise point positioning for the efficient and robust analysis of GPS data from large networks. *J. Geophys. Res. Solid Earth* **1997**, *102*, 5005–5017. [[CrossRef](#)]
5. Kouba, J.; Héroux, P. Precise point positioning using IGS orbit and clock products. *GPS Solut.* **2001**, *5*, 12–28. [[CrossRef](#)]
6. Gao, Y.; Shen, X. A New Method for Carrier-Phase-Based Precise Point Positioning. *Navigation* **2002**, *49*, 109–116. [[CrossRef](#)]
7. Abdel-Salam, M.A.-T. *Precise Point Positioning using Un-Differenced Code and Carrier Phase Observations*; University of Calgary: Calgary, AB, Canada, 2005; Volume 69. Available online: https://www.collectionscanada.gc.ca/obj/thesescanada/vol2/002/NR37676.PDF?is_thesis=1&oclc_number=302053384 (accessed on 17 October 2022).
8. Dow, J.M.; Neilan, R.E.; Rizos, C. The international GNSS service in a changing landscape of global navigation satellite systems. *J. Geod.* **2009**, *83*, 191–198. [[CrossRef](#)]
9. Ogutcu, S. Performance assessment of IGS combined/JPL individual rapid and ultra-rapid products: Consideration of Precise Point Positioning technique. *Int. J. Eng. Geosci.* **2020**, *5*, 1–14. [[CrossRef](#)]
10. Chu, C.-W.; Chiang, Y.-T.; Chang, F.-R.; Wang, H.-S. Toward real-time precise point positioning: Differential GPS based on IGS ultra rapid product. In Proceedings of the SICE Annual Conference, Taipei, Taiwan, 18–21 August 2010; pp. 355–358.
11. Chen, J.; Li, H.; Wu, B.; Zhang, Y.; Wang, J.; Hu, C. Performance of real-time precise point positioning. *Mar. Geod.* **2013**, *36*, 98–108. [[CrossRef](#)]
12. Duan, B.; Hugentobler, U.; Chen, J.; Selmke, I.; Wang, J. Prediction versus real-time orbit determination for GNSS satellites. *GPS Solut.* **2019**, *23*, 39. [[CrossRef](#)]
13. Pan, L.; Gao, X.; Hu, J.; Ma, F.; Zhang, Z.; Wu, W. Performance assessment of real-time multi-GNSS integrated PPP with uncombined and ionospheric-free combined observables. *Adv. Space Res.* **2021**, *67*, 234–252. [[CrossRef](#)]
14. Caissy, M.; Agrotis, L.; Weber, G.; Fisher, S. The IGS real-time service. In Proceedings of the EGU General Assembly Conference Abstracts, Vienna, Austria, 7–12 April 2013; p. EGU2013-11168.
15. Weber, G.; Mervart, L.; Lukes, Z.; Rocken, C.; Dousa, J. Real-time clock and orbit corrections for improved point positioning via NTRIP. In Proceedings of the 20th international technical meeting of the satellite division of the institute of navigation (ION GNSS 2007), Fort Worth, TX, USA, 25–28 September 2007; pp. 1992–1998.
16. Elsobeiey, M.; Al-Harbi, S. Performance of real-time Precise Point Positioning using IGS real-time service. *GPS Solut.* **2016**, *20*, 565–571. [[CrossRef](#)]
17. Li, Z.; Zhang, J.; Li, T.; He, X.; Wu, M. Analysis of static and dynamic real-time precise point positioning and precision based on SSR correction. In Proceedings of the 2016 IEEE International Conference on Information and Automation (ICIA), Ningbo, China, 1–3 August 2016; pp. 2022–2027.
18. Wang, Z.; Li, Z.; Wang, L.; Wang, X.; Yuan, H. Assessment of multiple GNSS real-time SSR products from different analysis centers. *ISPRS Int. J. Geo-Inf.* **2018**, *7*, 85. [[CrossRef](#)]
19. Ouyang, C.; Shi, J.; Huang, Y.; Guo, J.; Xu, C. Evaluation of BDS-2 real-time orbit and clock corrections from four IGS analysis centers. *Measurement* **2021**, *168*, 108441. [[CrossRef](#)]
20. Ge, Y.; Chen, S.; Wu, T.; Fan, C.; Qin, W.; Zhou, F.; Yang, X. An analysis of BDS-3 real-time PPP: Time transfer, positioning, and tropospheric delay retrieval. *Measurement* **2021**, *172*, 108871. [[CrossRef](#)]
21. Lu, X.; Chen, L.; Shen, N.; Wang, L.; Jiao, Z.; Chen, R. Decoding PPP corrections from BDS B2b signals using a software-defined receiver: An initial performance evaluation. *IEEE Sens. J.* **2020**, *21*, 7871–7883. [[CrossRef](#)]
22. Nie, Z.; Xu, X.; Wang, Z.; Du, J. Initial assessment of BDS PPP-B2b service: Precision of orbit and clock corrections, and PPP performance. *Remote Sens.* **2021**, *13*, 2050. [[CrossRef](#)]
23. Tao, J.; Liu, J.; Hu, Z.; Zhao, Q.; Chen, G.; Ju, B. Initial Assessment of the BDS-3 PPP-B2b RTS compared with the CNES RTS. *GPS Solut.* **2021**, *25*, 131. [[CrossRef](#)]
24. Xu, Y.; Yang, Y.; Li, J. Performance evaluation of BDS-3 PPP-B2b precise point positioning service. *GPS Solut.* **2021**, *25*, 142. [[CrossRef](#)]
25. Ren, Z.; Gong, H.; Peng, J.; Tang, C.; Huang, X.; Sun, G. Performance assessment of real-time precise point positioning using BDS PPP-B2b service signal. *Adv. Space Res.* **2021**, *68*, 3242–3254. [[CrossRef](#)]
26. BeiDou Navigation Satellite System Signal in Space Interface Control Document: Precise Point Positioning Service Signal PPP-B2b (Version 1.0). 2020. Available online: <http://en.beidou.gov.cn/SYSTEMS/ICD/202008/P020200803538771492778.pdf> (accessed on 20 October 2021).
27. Hadas, T.; Bosy, J. IGS RTS precise orbits and clocks verification and quality degradation over time. *GPS Solut.* **2015**, *19*, 93–105. [[CrossRef](#)]
28. Ge, M.; Chen, J.; Douša, J.; Gendt, G.; Wickert, J. A computationally efficient approach for estimating high-rate satellite clock corrections in realtime. *GPS Solut.* **2012**, *16*, 9–17. [[CrossRef](#)]
29. Li, X.; Ge, M.; Dai, X.; Ren, X.; Fritsche, M.; Wickert, J.; Schuh, H. Accuracy and reliability of multi-GNSS real-time precise positioning: GPS, GLONASS, BeiDou, and Galileo. *J. Geod.* **2015**, *89*, 607–635. [[CrossRef](#)]
30. Gao, Z.; Zhang, H.; Ge, M.; Niu, X.; Shen, W.; Wickert, J.; Schuh, H. Tightly coupled integration of multi-GNSS PPP and MEMS inertial measurement unit data. *GPS Solut.* **2017**, *21*, 377–391. [[CrossRef](#)]
31. An, X.; Meng, X.; Jiang, W. Multi-constellation GNSS precise point positioning with multi-frequency raw observations and dual-frequency observations of ionospheric-free linear combination. *Satell. Navig.* **2020**, *1*, 7. [[CrossRef](#)]

32. Guo, F.; Zhang, X.; Wang, J. Timing group delay and differential code bias corrections for BeiDou positioning. *J. Geod.* **2015**, *89*, 427–445. [[CrossRef](#)]
33. Gao, Z.; Ge, M.; Shen, W.; Zhang, H.; Niu, X. Ionospheric and receiver DCB-constrained multi-GNSS single-frequency PPP integrated with MEMS inertial measurements. *J. Geod.* **2017**, *91*, 1351–1366. [[CrossRef](#)]
34. Jin, S.; Su, K. PPP models and performances from single-to quad-frequency BDS observations. *Satell. Navig.* **2020**, *1*, 16. [[CrossRef](#)]
35. Zhang, B.; Zhao, C.; Odolinski, R.; Liu, T. Functional model modification of precise point positioning considering the time-varying code biases of a receiver. *Satell. Navig.* **2021**, *2*, 11. [[CrossRef](#)]
36. Weber, G.; Mervart, L.; Stuerze, A.; Rülke, A.; Stöcker, D. *BKG Ntrip Client (BNC), Version 2.12*; Mitteilungen des Bundesamtes für Kartographie und Geodäsie: Frankfurt am Main, Germany, 2016.
37. Kazmierski, K.; Zajdel, R.; Sośnica, K. Evolution of orbit and clock quality for real-time multi-GNSS solutions. *GPS Solut.* **2020**, *24*, 111. [[CrossRef](#)]
38. Lv, Y.; Geng, T.; Zhao, Q.; Xie, X.; Zhou, R. Initial assessment of BDS-3 preliminary system signal-in-space range error. *GPS Solut.* **2019**, *24*, 16. [[CrossRef](#)]
39. Blewitt, G. Carrier phase ambiguity resolution for the Global Positioning System applied to geodetic baselines up to 2000 km. *J. Geophys. Res. Solid Earth* **1989**, *94*, 10187–10203. [[CrossRef](#)]
40. Liu, Y.; Yang, C.; Zhang, M. Comprehensive Analyses of PPP-B2b Performance in China and Surrounding Areas. *Remote Sens.* **2022**, *14*, 643. [[CrossRef](#)]